

# PALLADIUM ISOTOPIC EVIDENCE FOR NUCLEOSYNTHETIC AND COSMOGENIC ISOTOPE ANOMALIES IN IVB IRON METEORITES

BERNHARD MAYER<sup>1</sup>, NADINE WITTIG<sup>1,2</sup>, MUNIR HUMAYUN<sup>1</sup>, AND INGO LEYA<sup>3</sup>

<sup>1</sup> National High Magnetic Field Laboratory and Department of Earth, Ocean & Atmospheric Science, Florida State University, 1800 E. Paul Dirac Drive, Tallahassee, FL 32310, USA

<sup>2</sup> Department of Earth Sciences, Carleton University, 1125 Colonel By Drive, Ottawa, K1S 5B6 Ontario, Canada

<sup>3</sup> Space Science and Planetology, Institute of Physics, University of Bern, Sidlerstrasse 5, 3012 Bern, Switzerland

Received 2015 March 27; accepted 2015 July 16; published 2015 August 21

## ABSTRACT

The origin of ubiquitous nucleosynthetic isotope anomalies in meteorites may represent spatial and/or temporal heterogeneity in the sources that supplied material to the nascent solar nebula, or enhancement by chemical processing. For elements beyond the Fe peak, deficits in s-process isotopes have been reported in some (e.g., Mo, Ru, W) but not all refractory elements studied (e.g., Os) that, among the iron meteorites, are most pronounced in IVB iron meteorites. Palladium is a non-refractory element in the same mass region as Mo and Ru. In this study, we report the first precise Pd isotopic abundances from IVB irons to test the mechanisms proposed for the origin of isotope anomalies. First, this study determined the existence of a cosmogenic neutron dosimeter from the reaction  $^{103}\text{Rh}(n, \beta^-)^{104}\text{Pd}$  in the form of excess  $^{104}\text{Pd}$ , correlated with excess  $^{192}\text{Pt}$ , in IVB irons. Second, all IVB irons show a deficit of the s-process only isotope  $^{104}\text{Pd}$  ( $\epsilon^{104}\text{Pd} = -0.48 \pm 0.24$ ), an excess of the r-only isotope  $^{110}\text{Pd}$  ( $\epsilon^{110}\text{Pd} = +0.46 \pm 0.12$ ), and no resolvable anomaly in the p-process  $^{102}\text{Pd}$  ( $\epsilon^{102}\text{Pd} = +1 \pm 1$ ). The magnitude of the Pd isotope anomaly is about half that predicted from a uniform depletion of the s-process yields from the correlated isotope anomalies of refractory Mo and Ru. The discrepancy is best understood as the result of nebular processing of the less refractory Pd, implying that all the observed nucleosynthetic anomalies in meteorites are likely to be isotopic relicts. The Mo–Ru–Pd isotope systematics do not support enhanced rates of the  $^{22}\text{Ne}(\alpha, n)^{25}\text{Mg}$  neutron source for the solar system s-process.

*Key words:* planetary nebulae: general – protoplanetary disks

## 1. INTRODUCTION

Nucleosynthetic isotope anomalies have been reported in Ti, Cr, Ni, Zr, Mo, Ru, Ba, Nd, Sm, W, and Os in samples of bulk chondritic meteorites that may indicate the provenance of protosolar material, reprocessed and incorporated during the formation of early solar system bodies (Yin et al. 2002; Dauphas et al. 2004; Markowski et al. 2006a, 2006b; Carlson et al. 2007; Qin et al. 2008; Regelous et al. 2008; Schönbachler et al. 2008; Trinquier et al. 2009; Chen et al. 2010; Burkhardt et al. 2011; Brennecka et al. 2012; Walker 2012; Wittig et al. 2013a; Akram et al. 2015). Even more enigmatic is the presence of nucleosynthetic isotope anomalies in asteroidal bodies that were large enough to melt and separate into cores and mantles. Among these differentiated planetesimals IVB iron meteorites exhibit the largest nucleosynthetic isotope effects in Mo, Ru, and W, but show no measurable isotope anomalies in Os (Qin et al. 2008; Chen et al. 2010; Burkhardt et al. 2011; Walker 2012; Wittig et al. 2013a). The observed nucleosynthetic anomalies in iron meteorites indicate a systematic s-process deficit on a planetary scale, an effect best seen in Mo and Ru isotopes (Chen et al. 2010; Burkhardt et al. 2011). It has been suggested that these deficits are the result of inefficient mixing of the presolar dust with inhomogeneous distribution of presolar grains (e.g., SiC; Dauphas et al. 2004), a late injection of fresh s-process material from an AGB star (e.g., Vanhala & Boss 2001) or the thermal or physical processing of the phases carrying these isotopic anomalies (Regelous et al. 2008; Trinquier et al. 2009; Burkhardt et al. 2012). The observed anomalies in iron meteorites have all been described in refractory elements (Mo, Ru, W) consistent with thermal processing. Molybdenum,

Ru, and W are known to partition into carbides, and Mo and Ru are present in substantial amounts in presolar SiC (Kashiv et al. 2002) that exhibit large s-process nucleosynthetic anomalies in Mo and Ru (e.g., Nicolussi et al. 1998; Savina et al. 2004).

To test whether carbide formation or the refractory character are essential in explaining the s-process deficits in IVB irons, and by inference other differentiated material, we have analyzed the isotopic composition of Pd in 10 different iron meteorites from group IVB. Palladium is a siderophile (iron-loving) element, that is not refractory (50% $T_c$ : 1324 K; Lodders 2003), condensing together with Fe, does not readily form carbides, and is absent from presolar SiC grains (Kashiv et al. 2002). Palladium has the p-only isotope  $^{102}\text{Pd}$ , the s-only isotope  $^{104}\text{Pd}$ , the r-only isotope  $^{110}\text{Pd}$ , and three isotopes ( $^{105}\text{Pd}$ ,  $^{106}\text{Pd}$ ,  $^{108}\text{Pd}$ ) of mixed s- and r-process origin (Figure 1). Thus, Pd in bulk iron meteorites would lack isotope anomalies if SiC inherited from low-mass AGB stars (Savina et al. 2004) is the main carrier of such anomalies. Since the largest Mo and Ru isotope anomalies were reported in IVB irons, we chose to focus on this group. Further, rigorous proof of an isotope anomaly is best demonstrated by analyzing multiple members of a single iron meteorite group, all members of which should share the same nucleosynthetic anomaly.

The IVB irons are a well-studied group (Campbell & Humayun 2005; Walker et al. 2008), with members recording considerable galactic cosmic-ray (GCR) exposure (Voshage 1984). Secondary neutrons produced by GCR irradiation of these irons are captured by nuclides creating isotopic shifts that are specific to the geometry and size of each studied meteorite specimen and cannot be taken as representative

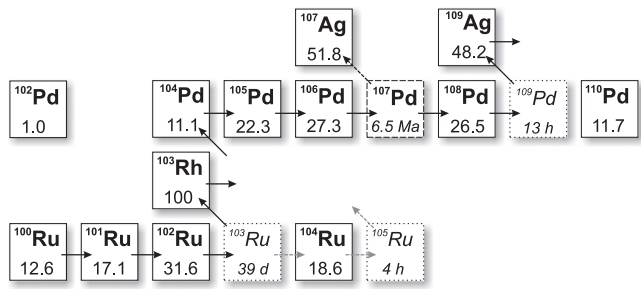


**Figure 1.** Schematic illustration of the nucleosynthetic processes that produced the Pd isotopes with the s-process pathway indicated by arrows. Stable isotopes are shown in bold with abundances (%) in solid boxes; short-lived radioisotopes are shown in italics with half-lives in millions of years (Ma), days (d), or hours (h) in dotted outlined boxes. The long-lived  $^{107}\text{Pd}$  isotope is shown separately. P-process only:  $^{102}\text{Pd}$ ; s-process only:  $^{104}\text{Pd}$ ; r-process only:  $^{110}\text{Pd}$ ; other isotopes are mixed s, r process.

of the IVB iron group as a whole. Wittig et al. (2013a) and Kruijjer et al. (2013, 2014) found that the reaction  $^{191}\text{Ir}(n, \beta^-)^{192}\text{Pt}$  produces a substantial isotope anomaly in  $\epsilon^{192}\text{Pt}$  that can be used as an in situ neutron dosimeter to correct the effects of neutron capture on other nuclides. Further, due to the high neutron capture cross-section of  $^{103}\text{Rh}$  (Mughabghab 2003), the reaction  $^{103}\text{Rh}(n, \beta^-)^{104}\text{Pd}$  has potential to produce observable effects in  $\epsilon^{104}\text{Pd}$  (Leya & Masarik 2013). Among the iron meteorites, the IVB irons show the most variability of GCR damage with Tlacotepec being the most irradiated and Tawallah Valley being among the least irradiated members (Kruijjer et al. 2013; Wittig et al. 2013a), which correspond to their GCR exposure ages of 945 Ma and 250 Ma, respectively (Voshage 1984).

In this study, we show the first precise Pd isotope compositions of IVB irons. We report the discovery of a clearly resolved cosmogenic effect on  $\epsilon^{104}\text{Pd}$  correlated with the in situ neutron dosimeter  $\epsilon^{192}\text{Pt}$  determined on the same irons (Wittig et al. 2013a), and a measurable nucleosynthetic anomaly in Pd isotopic composition as a group property of IVB irons. The GCR neutron capture effects on Rh in these IVB irons were modeled to examine the extent of the cosmogenic effect in  $\epsilon^{104}\text{Pd}$ , and are shown together with our new data. We explore the consequences of the Pd nucleosynthetic anomaly in the context of the various hypotheses to explain nuclear anomalies reported in meteorites.

## 2. ANALYTICAL METHODOLOGY

Palladium aliquots of five samples (Tlacotepec, Iquique, Tinnie, Skookum-2, Warburton Range-2) studied here were taken from the very same digestion as used in the Pt–Os–W isotope study by Wittig et al. (2013a), with the chemical separation described in Wittig et al. (2013a, 2013b) following a cleanup chemical procedure on a cation column. For the other five samples used in this study, either additional samples, or freshly cut pieces of iron metal adjacent to the specimens previously studied by Wittig et al. (2013a, 2013b) were processed in a similar manner. The chemical separation procedure of Pd was modified from Wittig et al. (2013a) collecting the Pd fraction off the anion column in HCl instead of  $\text{HNO}_3$  to avoid high Pt yields in the Pd fraction. For freshly dissolved iron meteorites, prior to separation of Pd by anion exchange chromatography, the Fe–Co–Ni matrix was removed with a cation-exchange column (AG<sup>®</sup> 50W-X8). Other isobaric

and molecular interferences (Mo, Ru, Cd, Zr, Zn, Yb, Ga, and Pt etc.) were removed using an anion-exchange column (AG<sup>®</sup> 1-X8). Isotope measurements were made during six sessions on the Thermo Neptune<sup>™</sup>MC-ICP-MS (at the Plasma Analytical Facility, NHMFL) using 100 ng/mL Pd solutions in 2% HCl with an ESI Apex<sup>™</sup> introduction system or with an ESI SIS<sup>™</sup> spray chamber using Thermo SuperJet8.3 Ni sampler and Spectron T1001Ni-X skimmer cones. The cup configuration used was  $^{101}\text{Ru}$  (L4),  $^{102}\text{Pd}$  (L3),  $^{103}\text{Rh}$  (L2),  $^{104}\text{Pd}$  (L1),  $^{105}\text{Pd}$  (C),  $^{106}\text{Pd}$  (H1),  $^{108}\text{Pd}$  (H2),  $^{110}\text{Pd}$  (H3), and  $^{111}\text{Cd}$  (H4) with 240 replicate measurements taken in static mode. The Pd ratios were normalized to  $^{108}\text{Pd}/^{105}\text{Pd} = 1.18899$  (Kelly & Wasserburg 1978) using the exponential law for instrumental mass bias correction. The Pd isotope composition is reported in epsilon notation referenced to the terrestrial Pd solution (Alfa Aesar, Pd high purity standard solution). Typical within-session reproducibility for  $\epsilon^{102}\text{Pd}$ ,  $\epsilon^{104}\text{Pd}$ ,  $\epsilon^{106}\text{Pd}$ , and  $\epsilon^{110}\text{Pd}$  was  $\pm 0.62$ ,  $\pm 0.20$ ,  $\pm 0.10$ , and  $\pm 0.13 \epsilon u$ , respectively.

Isobaric Ru and Cd interferences on Pd were monitored via signals at mass 101 ( $^{101}\text{Ru}$ ) and 111 ( $^{111}\text{Cd}$ ). Corrections for Cd interferences were negligible (Figures 2, 3). To assess the degree to which isobaric interferences from Ru could be reliably corrected, Ru-doped Pd solutions were analyzed for their Pd isotopic composition which showed that a  $^{101}\text{Ru}/^{105}\text{Pd}$  ratio higher than 0.009 resulted in insufficient correction of  $^{102}\text{Ru}$  on  $^{102}\text{Pd}$  and  $^{101}\text{Ru}/^{105}\text{Pd}$  ratios higher than 0.02 resulted in insufficient correction of  $^{104}\text{Ru}$  on  $^{104}\text{Pd}$  (Figure 3). Possible molecular interferences from  $\text{ZrO}^+$ ,  $\text{ZnAr}^+$  and  $\text{NiAr}^+$ , etc., were monitored prior to MC-ICP-MS analysis using a single collector ICP-MS (Thermo Element2<sup>™</sup>), and an additional cation-exchange clean-up column was applied to lower these interferences to negligible levels before analyzing the solutions for Pd isotope composition. For three samples with ZrO interferences (affected masses: 106, 107, 108, 110) additional corrections have been applied. Although the  $\text{ZrO}^+$  does not interfere with  $^{104}\text{Pd}$ , the mass bias correction propagates the interference on  $^{108}\text{Pd}$  to all Pd isotope ratios, with the largest effect on  $\epsilon^{106}\text{Pd}$ .  $^{106}\text{Pd}$  has s- and r-process contributions intermediate between  $^{108}\text{Pd}$  and  $^{105}\text{Pd}$  and, therefore, will not show pronounced anomalies resulting from nucleosynthetic processes. In addition, cosmogenic effects are small and more pronounced on  $^{105}\text{Pd}$  (negative) and  $^{108}\text{Pd}$  (positive) than on  $^{106}\text{Pd}$ . Therefore, with the instrumental mass bias correction of  $^{108}\text{Pd}/^{105}\text{Pd}$  neither cosmogenic nor nucleosynthetic effects can produce significant anomalies for the resulting  $\epsilon^{106}\text{Pd}$ . Since neither cosmogenic nor nucleosynthetic processes affect  $\epsilon^{106}\text{Pd}$  significantly it becomes a sensitive monitor for  $\text{ZrO}^+$  interferences. Measurements of a Zr-doped Pd standard solution were used to define a relationship between each Pd isotope ratio and  $\epsilon^{106}\text{Pd}$  due to  $\text{ZrO}^+$  interference alone, and the  $\epsilon$  values for the three irons for which corrections were necessary were corrected assuming  $\epsilon^{106}\text{Pd} = 0$  (Figure 4). The robustness and accuracy of this correction procedure was assessed by comparison with replicate measurements of the same sample in which no Zr interference correction was necessary (e.g., Warburton Range-1, Skookum-1).

## 3. RESULTS

The Pd isotope compositions of the 10 studied IVB iron meteorites are given in Table 1 together with the 2 standard errors for each set of measurements (Here, and elsewhere,

**Table 1**  
Pd Isotopic Data for IVB Iron Meteorites and Measured Ru/Pd Ratio after Separation

	Rh/Pd <sup>a</sup>	<sup>101</sup> Ru/ <sup>105</sup> Pd	$\epsilon^{102}\text{Pd}$	2SE <sup>c</sup>	$\epsilon^{104}\text{Pd}^b$	2SE <sup>c</sup>	$\epsilon^{106}\text{Pd}$	2SE	$\epsilon^{110}\text{Pd}$	2SE	Sample Introduction
Warburton-1	...	0.0134	2.1	$\pm 1.7$	-0.43	$\pm 0.54$	-0.10	$\pm 0.17$	0.42	$\pm 0.19$	SIS
Warburton-2	...	0.0013	1.7	$\pm 2.1$	-0.45	$\pm 0.34$	...	...	0.44	$\pm 0.11$	APEX
Mean	0.4	...	1.7	$\pm 2.1$	-0.44	$\pm 0.29$	-0.10	$\pm 0.17$	0.43	$\pm 0.10$	...
Tinnie	0.4	0.0055	1.6	$\pm 0.8$	-0.29	$\pm 0.16$	-0.06	$\pm 0.06$	0.47	$\pm 0.14$	APEX
Skookum-1	...	0.0078	2.6	$\pm 1.4$	-0.28	$\pm 0.30$	-0.19	$\pm 0.11$	0.45	$\pm 0.12$	SIS
Skookum-2	...	0.0009	1.2	$\pm 0.3$	-0.27	$\pm 0.11$	-0.01	$\pm 0.04$	0.55	$\pm 0.07$	APEX
Mean	0.4	...	1.3	$\pm 0.3$	-0.27	$\pm 0.10$	-0.03	$\pm 0.03$	0.53	$\pm 0.06$	...
Tawallah Valley	0.4	0.0265	<i>37.1</i>	$\pm 6.9$	-0.14	$\pm 0.82$	0.05	$\pm 0.09$	0.45	$\pm 0.15$	SIS
Hoba-1a	...	0.0003	2.7	$\pm 1.5$	-0.10	$\pm 0.39$	0.04	$\pm 0.10$	0.51	$\pm 0.59$	APEX
Hoba-1b	...	0.0003	2.3	$\pm 0.6$	-0.09	$\pm 0.31$	-0.01	$\pm 0.06$	0.60	$\pm 0.40$	APEX
Hoba-2a	...	0.0003	1.4	$\pm 1.0$	-0.23	$\pm 0.47$	-0.17	$\pm 0.11$	0.60	$\pm 0.62$	APEX
Hoba-2b	...	0.0003	2.5	$\pm 0.5$	-0.22	$\pm 0.39$	0.07	$\pm 0.09$	0.46	$\pm 0.46$	APEX
Mean	0.6	...	2.3	$\pm 0.4$	-0.15	$\pm 0.19$	-0.01	$\pm 0.04$	0.55	$\pm 0.25$	...
Santa Clara	0.5	0.0051	2.4	$\pm 9.7$	0.01	$\pm 1.06$	-0.01	$\pm 0.31$	0.58	$\pm 0.51$	SIS
Dumont	0.6	0.0027	1.1	$\pm 2.2$	0.18	$\pm 0.24$	0.03	$\pm 0.07$	0.55	$\pm 0.15$	SIS
Iquique	0.6	0.0019	1.5	$\pm 1.4$	0.23	$\pm 0.17$	...	...	0.48	$\pm 0.12$	APEX
Kokomo-1	...	0.00002	1.8	$\pm 0.5$	0.38	$\pm 0.08$	0.06	$\pm 0.05$	0.49	$\pm 0.09$	SIS
Kokomo-2a	...	0.00003	0.8	$\pm 0.2$	0.47	$\pm 0.16$	0.18	$\pm 0.06$	0.23	$\pm 0.14$	APEX
Kokomo-2b	...	0.00003	0.2	$\pm 0.2$	0.36	$\pm 0.16$	-0.02	$\pm 0.05$	0.39	$\pm 0.06$	APEX
Mean	0.7	...	0.6	$\pm 0.2$	0.39	$\pm 0.07$	0.06	$\pm 0.03$	0.40	$\pm 0.05$	...
Tlacotepec	0.6	0.0044	0.9	$\pm 2.6$	1.05	$\pm 0.14$	...	...	0.53	$\pm 0.14$	APEX

**Notes.** Samples are listed in order of ascending  $\epsilon^{192}\text{Pt}$  (Wittig et al. 2013a). *Italic font* represents values with high Ru corrections; the missing value for  $\epsilon^{106}\text{Pd}$  has been used for Zr correction, see text for further discussion. Number after meteorite names represents dissolution of separate piece of iron; letters after number represent replicate analyses of the same sample solution. Normalized to  $^{108}\text{Pd}/^{105}\text{Pd} = 1.18899$  (Kelly & Wasserburg 1978) using the exponential law, errors are in-run 2 standard errors.

<sup>a</sup> Elemental concentrations from Walker et al. (2008).

<sup>b</sup> Note that  $\epsilon^{104}\text{Pd}$  is not GCR corrected.

<sup>c</sup> Propagated error, integrating the influence of the Ru correction.

errors are reported as  $2\sigma$ ). In Table 1, numbers after meteorite names represent separate replicate analyses and digestions of metal cuts from the same piece of iron and processed separately through the full chemical separation procedure; letters after numbers (a, b) represent replicate analyses of the same sample solution processed once through the chemical separation procedure. The average of duplicates is reported using the error weighted mean with  $2\sigma$  standard deviation. In the case of Warburton Range-1 and Tawallah Valley, the  $^{101}\text{Ru}/^{105}\text{Pd}$  ratio is higher than 0.009 and, therefore,  $\epsilon^{102}\text{Pd}$  could not be adequately corrected. In this study, due to the large Ru isobaric corrections required,  $\epsilon^{102}\text{Pd}$  is not measured sufficiently precisely to provide useful constraints on models of nucleosynthetic anomalies so it will not be discussed further. For samples Warburton Range-2, Iquique, and Tlacotepec, significant Zr contribution as  $^{90}\text{Zr}^{16}\text{O}$  required corrections that set  $\epsilon^{106}\text{Pd} = 0$ .

For the sample Skookum-2, mass 107 ( $^{91}\text{Zr}^{16}\text{O}$ ) was also measured. Using natural isotope abundances of Zr and observed mass bias on Pd the interferences from  $\text{ZrO}^+$  on the masses 106, 108, and 110 could then be corrected without assuming a value for  $\epsilon^{106}\text{Pd}$ . These corrected  $\epsilon^{104}\text{Pd}$ ,  $\epsilon^{106}\text{Pd}$ , and  $\epsilon^{110}\text{Pd}$  values agree with a duplicate of that sample (Skookum-1) which had negligible Zr interferences. For the samples Warburton Range-2, Iquique, and Tlacotepec, we used the observed shift in a Zr-doped Pd standard solution to correct the effect of Zr as described above. For a first order test of that approach we compared the results with corrections based on the Zr/Pd ratio measurements from elemental abundance determinations. Using natural isotope abundances of Zr, the observed

mass bias scaled from Pd and an oxide production rate of  $^{90}\text{Zr}^{16}\text{O}^+ / ^{90}\text{Zr}^+$  of 0.8% (as observed in Skookum-2) the corrected values for  $\epsilon^{104}\text{Pd}$  and  $\epsilon^{110}\text{Pd}$  agree within errors with the previous correction approach. In addition, the duplicate analysis, Warburton Range-1, with negligible Zr interference is within error of the interference-corrected values for Warburton Range-2, which demonstrates the robustness of the interference corrections applied here. Therefore, the  $\epsilon^{106}\text{Pd}$  of Tlacotepec and Iquique were not used and for Warburton Range only the  $\epsilon^{106}\text{Pd}$  without Zr interference was used for calculating the mean  $\epsilon^{106}\text{Pd}$  of the IVB meteorites.

The presence of a strong cosmogenic anomaly from the neutron capture of  $^{103}\text{Rh}$  is seen in  $\epsilon^{104}\text{Pd}$ , which is well correlated with  $\epsilon^{192}\text{Pt}$  from neutron capture on  $^{191}\text{Ir}$  in the IVB irons (Figure 5). For comparison, the  $\epsilon^{104}\text{Pd}$  versus  $\epsilon^{192}\text{Pt}$  calculated by the GCR model of Leya & Masarik (2013) is shown. In this model,  $\epsilon^i\text{Pd}$  shifts have been calculated for terrestrial initial Pd and Pt isotopic compositions at various meteoroid depths and sizes (0.01–1.25 m) with specific compositional inputs (Rh/Pd, Ir/Pt) and exposure ages for the IVB irons. Variations of the IVB irons in  $\epsilon^{104}\text{Pd}$  are well correlated with  $\epsilon^{192}\text{Pt}$  (Figure 5),  $\epsilon^{189}\text{Os}$  and  $\epsilon^{182}\text{W}$  (not shown), and define a slope that is parallel to that of the GCR model results, but displaced to a lower intercept ( $\epsilon^{104}\text{Pd} = -0.48 \pm 0.24$ ) at  $\epsilon^{192}\text{Pt} = 0$ . The error weighted mean for  $\epsilon^{106}\text{Pd}$  of 8 IVB samples is  $0.01 \pm 0.11$  (Tlacotepec and Iquique excluded). The measured IVB meteorites exhibit an error weighted mean for  $\epsilon^{110}\text{Pd}$  of  $0.46 \pm 0.12$ . Both individual  $\epsilon$ -values of  $\epsilon^{106}\text{Pd}$  and  $\epsilon^{110}\text{Pd}$  are weakly correlated with their measured  $\epsilon^{104}\text{Pd}$  (Figure 6(a), (b)) indicating that the

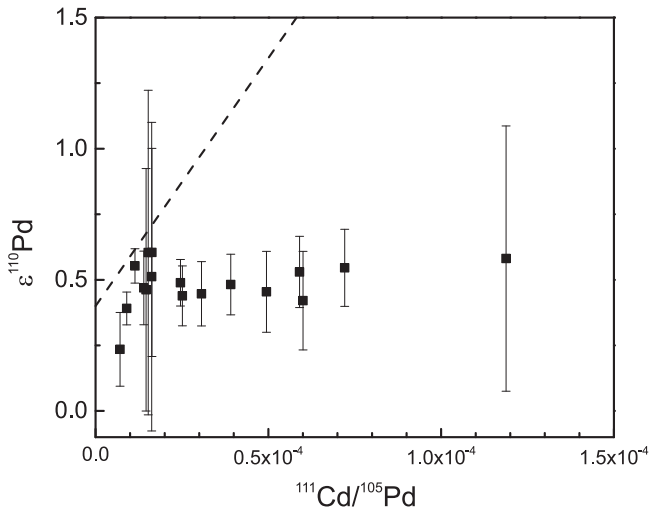


**Figure 2.** Correlation between the measured  $^{111}\text{Cd}/^{105}\text{Pd}$  ratio and the Cd interference-corrected  $\epsilon^{110}\text{Pd}$  for the IVB iron meteorites. The dashed line on the left represents the calculated  $\epsilon^{110}\text{Pd}$  without Cd isobaric correction but including the nucleosynthetic isotope anomaly in  $\epsilon^{110}\text{Pd}$ . The Cd corrections have a negligible effect on the measured Pd isotope ratios.

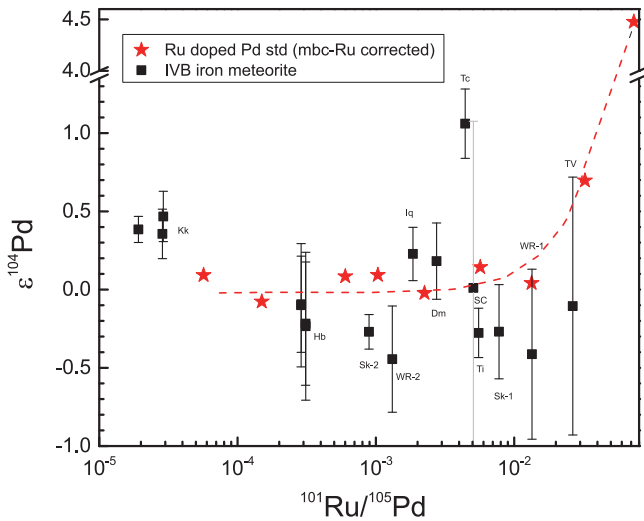


**Figure 3.** Correlation between the measured  $^{101}\text{Ru}/^{105}\text{Pd}$  ratio and the Ru-corrected  $\epsilon^{104}\text{Pd}$  for the IVB iron meteorites. Red stars represent the Ru-doped Pd standard solution that has been corrected using a mass biased  $^{101}\text{Ru}/^{104}\text{Ru}$  ratio. Samples with measured  $^{101}\text{Ru}/^{105}\text{Pd}$  ratios higher than 0.03 cannot be sufficiently corrected for isobaric interferences of Ru on  $^{104}\text{Pd}$ . Kk: Kokomo; Hb: Hoba; Sk: Skookum; WR: Warburton Range; Iq: Iquique; Dm: Dumont; Tc: Tlacotepec; SC: Santa Clara; Ti: Tinnie; TV: Tawallah Valley.

cosmogenic effect on these  $\epsilon$  values is less than  $0.1 \epsilon$  u which is consistent with the predictions of the GCR model of Leya & Masarik (2013; Figure 6).

## 4. DISCUSSION

### 4.1. Cosmogenic Effects

#### 4.1.1. Empirical Pd Isotope Data

Cosmogenic neutron capture effects have long been discussed in iron meteorites (e.g., Masarik 1997; Leya et al. 2000, 2003; Markowski et al. 2006a; Leya & Masarik 2013) specifically with respect to the application of the  $\epsilon^{182}\text{W}$  chronometer. Significant effects in IVB iron meteorites

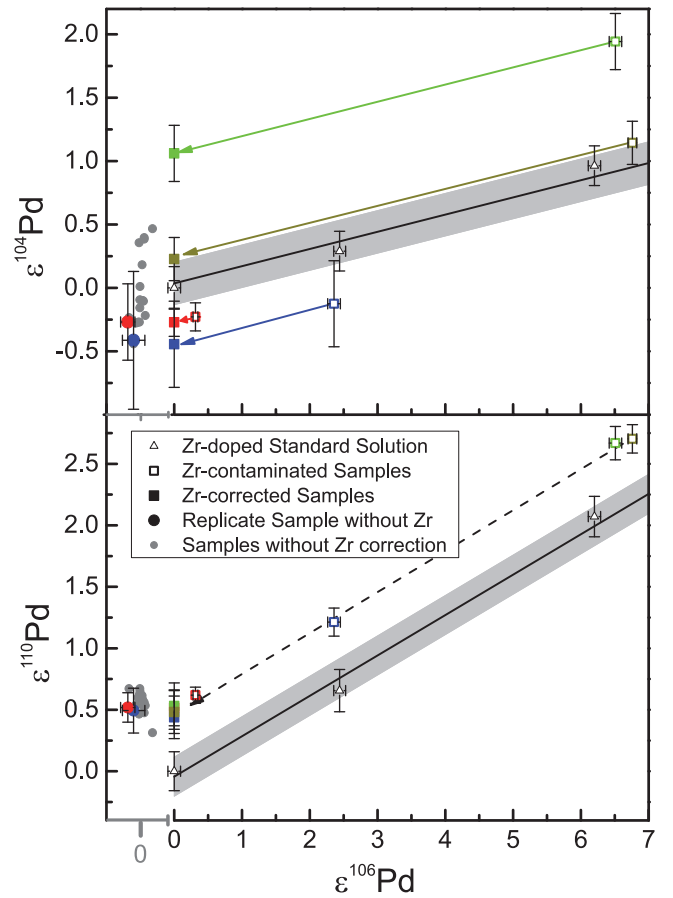


**Figure 4.** Effect of isobaric corrections for  $\text{ZrO}^+$  interferences. Measurements of Zr-doped Pd standard solutions (triangles) have been used to define the relationship between the Pd isotope ratios (solid line) and  $\epsilon^{106}\text{Pd}$  due to  $\text{ZrO}^+$  interference alone. The  $\epsilon$  values for irons (Tlacotepec green, Iquique dark yellow, Warburton Range-2 blue, and Skookum-2 red) are shown as open squares before isobaric correction, and the corrected values are shown as filled squares assuming  $\epsilon^{106}\text{Pd} = 0$ . Note that on the left side the replicate samples with negligible Zr interferences are plotted with a separate x-axis at the same scale together with other IVB irons (gray dots). Replicate analyses of samples with negligible Zr corrections, Warburton Range-1 and Skookum-1, are shown as red and blue circles for comparison with analyses (Warburton Range-2; Skookum-2) of the same meteorites with Zr corrections applied.

due to secondary neutron capture by the reaction  $^{191}\text{Ir}(n, \beta^-)^{192}\text{Pt}$  was demonstrated independently by Wittig et al. (2013a) and Kruijer et al. (2013), with effects as large as  $\sim 50 \epsilon$  u in  $\epsilon^{192}\text{Pt}$ . Since the neutron capture cross sections of Mo and Ru isotopes are small relative to that of  $^{103}\text{Rh}$ , GCR damage on those isotopes are negligible as shown by previous studies (Chen et al. 2010; Burkhardt et al. 2011). Thus, in the mass region between 90 and 110 the effects of GCR irradiation are prone to strongly effect  $^{104}\text{Pd}$  due to the reaction  $^{103}\text{Rh}(n, \beta^-)^{104}\text{Pd}$  (Leya & Masarik 2013). Here, we show the first empirical data to constrain the magnitude of the GCR irradiation for this reaction. In Figure 5, the  $\epsilon^{104}\text{Pd}$  correlates well with the recently established in situ neutron dosimeter of  $\epsilon^{192}\text{Pt}$  measured on the same irons (Wittig et al. 2013a) highlighting that ubiquitous secondary neutron capture reactions are recorded in IVB irons. Further, since  $\epsilon^{192}\text{Pt}$  is also correlated with  $\epsilon^{189}\text{Os}$  and  $\epsilon^{182}\text{W}$  (Wittig et al. 2013a), changes in each of these isotope ratios also correlate with  $\epsilon^{104}\text{Pd}$  in IVB irons.

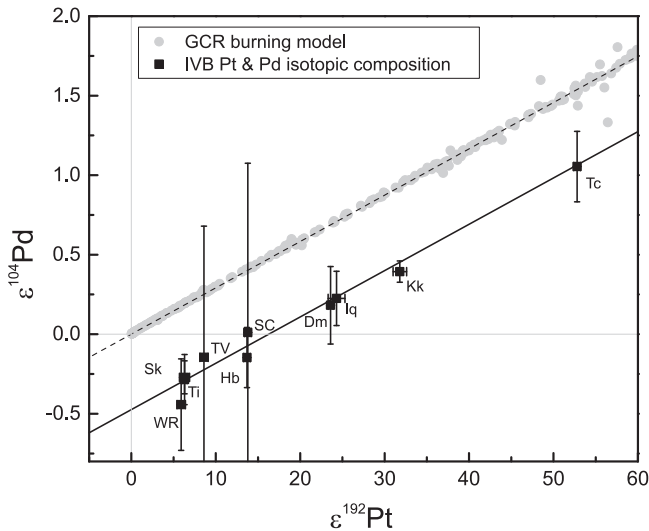


**Figure 5.** Comparison of  $\epsilon^{104}\text{Pd}$  with the in situ neutron dosimeter  $\epsilon^{192}\text{Pt}$  measured on the same samples of IVB iron meteorites (Wittig et al. 2013a) showing a strong cosmogenic increase in  $^{104}\text{Pd}$  from neutron capture on  $^{103}\text{Rh}$ . Black squares represent individual measurements of IVB iron meteorites (Table 1) and the black line is a linear regression through these data. Gray dots represent modeled effects of GCR reactions for iron meteorites with an exposure age of 945 Ma, Rh/Pd ratio of 0.6, and Ir/Pt of 1.03 (see the text for further details) and the dashed line is the cosmogenic production line. Note that the intercept for  $\epsilon^{104}\text{Pd}$  at  $\epsilon^{192}\text{Pt} = 0$  is  $-0.48 \epsilon u$  while the slope of the IVB irons is parallel to the cosmogenic production line. Kk: Kokomo; Hb: Hoba; Sk: Skookum; WR: Warburton Range; Iq: Iquique; Dm: Dumont; Tc: Tlacotepec; SC: Santa Clara; Ti: Tinnie; TV: Tawallah Valley.

#### 4.1.2. Numerical Estimates of Cosmogenic Pd Isotope Anomalies

Calculations with the model of Leya & Masarik (2013) using an exposure age of 950 Ma (Voshage 1984), a Rh/Pd ratio of 0.6 and a Ir/Pt ratio of 1.0 which is relevant to the composition of the most irradiated IVB iron Tlacotepec (Campbell & Humayun 2005; Walker et al. 2008), for different depths and radii indicate a positive correlation with a slope of 0.029 (Figure 5) between  $\epsilon^{192}\text{Pt}$  and  $\epsilon^{104}\text{Pd}$ . The same slope is seen in the  $\epsilon^{192}\text{Pt}$  versus  $\epsilon^{104}\text{Pd}$  space of the IVB iron meteorites ( $0.029 \pm 0.003$ ). Hence, Pt and Pd record the same GCR effect in the same samples indicating that Pd isotopes are a valuable in situ neutron dosimeter in irons that have sufficiently high Rh/Pd ratios. Importantly, using the correlation of  $\epsilon^{192}\text{Pt}-\epsilon^{104}\text{Pd}$ , the intercept of  $\epsilon^{104}\text{Pd}$  does not pass through the origin at  $\epsilon^{192}\text{Pt} = 0$ , which indicates the presence of a nucleosynthetic anomaly in  $\epsilon^{104}\text{Pd}$  (discussed further below).

For  $^{108}\text{Pd}/^{105}\text{Pd}$  normalized  $\epsilon$  values, the model also predicts small positive anomalies of  $\epsilon^{106}\text{Pd}$  and  $\epsilon^{110}\text{Pd}$  with around the same magnitude (for further details, see Leya & Masarik 2013). Figure 6 shows the correlation between  $\epsilon^{106}\text{Pd}$ ,  $\epsilon^{110}\text{Pd}$  and  $\epsilon^{104}\text{Pd}$  together with model estimates. A very weak correlation between  $\epsilon^{106}\text{Pd}$  and  $\epsilon^{104}\text{Pd}$  is observed suggesting a somewhat lower  $\epsilon^{106}\text{Pd}$  if GCR corrected than the given weighted mean of all samples. Due to the errors of each individual sample and the weak correlation we are not presenting GCR corrected data for  $\epsilon^{106}\text{Pd}$ . Virtually no correlation between  $\epsilon^{110}\text{Pd}$  and  $\epsilon^{104}\text{Pd}$  is observed. A nucleosynthetic anomaly in  $\epsilon^{110}\text{Pd}$  results in the intercept of this ratio being  $0.46 \epsilon u$  higher than the model prediction (Figures 2, 6), which assumed terrestrial Pd isotopic composition as the starting composition before cosmic-ray induced isotope shifts.

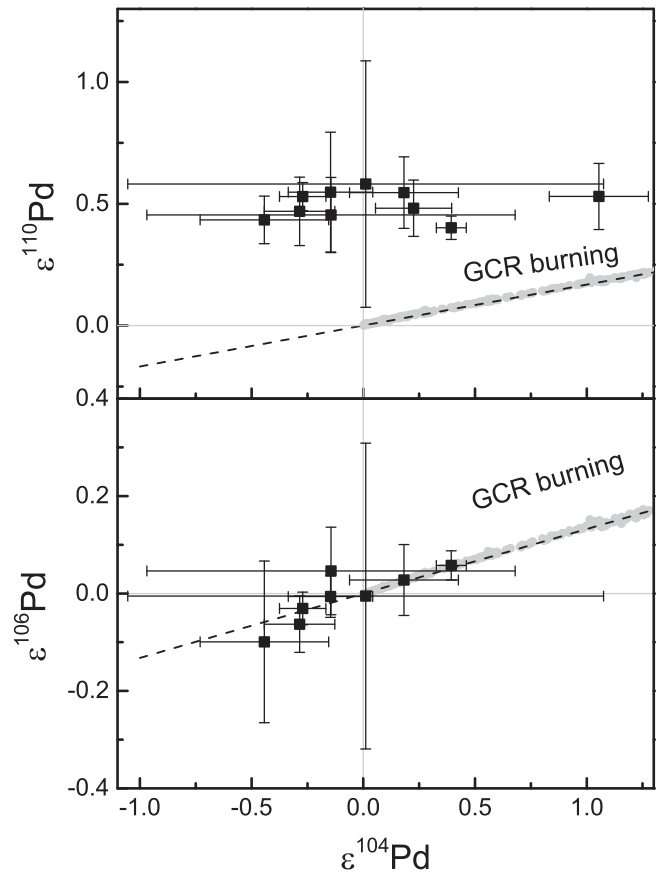


**Figure 6.** Observed variation of  $\epsilon^{110}\text{Pd}$  (above) and  $\epsilon^{106}\text{Pd}$  (lower figure) with  $\epsilon^{104}\text{Pd}$ , with the modeled cosmogenic effect shown as gray dots. Note that the IVB irons show initial negative anomalies in  $\epsilon^{104}\text{Pd}$  and distinct positive anomalies in  $\epsilon^{110}\text{Pd}$  not associated with cosmogenic effects.

#### 4.2. Nucleosynthetic Effects

Nucleosynthetic isotope anomalies are a property that is inherited from the parent asteroid from which an iron meteorite group chemically differentiated. Thus, for magmatic iron meteorites, it should be a property of every member of that group. This distinguishes nucleosynthetic isotope anomalies from cosmogenic isotope anomalies that are properties of an individual iron meteorite, being functions of its exposure age and depth inside the irradiated body. The GCR corrected  $\epsilon^{104}\text{Pd}$  for IVB irons exhibits a well-resolved negative anomaly ( $-0.48 \pm 0.24 \epsilon u$ ) consistently in all IVB irons analyzed (Figure 5). Since the isotope  $^{104}\text{Pd}$  is the s-only isotope for Pd this negative anomaly indicates an s-process deficit or an r-process excess recorded in these IVB iron meteorites. Figure 7 shows the average Pd isotope composition of IVB irons (corrected for GCR effects) compared with predictions for nucleosynthetic s-process deficits or r-process excesses relative to solar abundances. Using s-process yields from AGB stellar or galactic chemical evolution (GCE) models (Arlandini et al. 1999; Bisterzo et al. 2011, 2014) a s-deficit of  $-0.48$  on  $\epsilon^{104}\text{Pd}$  should, in turn, result in a positive anomaly of about  $0.44 \epsilon u$  for  $\epsilon^{110}\text{Pd}$  and a slightly negative anomaly in  $\epsilon^{106}\text{Pd}$  of  $-0.09 \epsilon u$  (Figure 7). Modeled curves for a Pd isotope s-process deficit or r-process excess are calculated from two distinct estimates of the AGB stellar model s-process yields (Arlandini et al. 1999; Bisterzo et al. 2015) which yielded nearly identical effects (Figure 7). Variations of the input

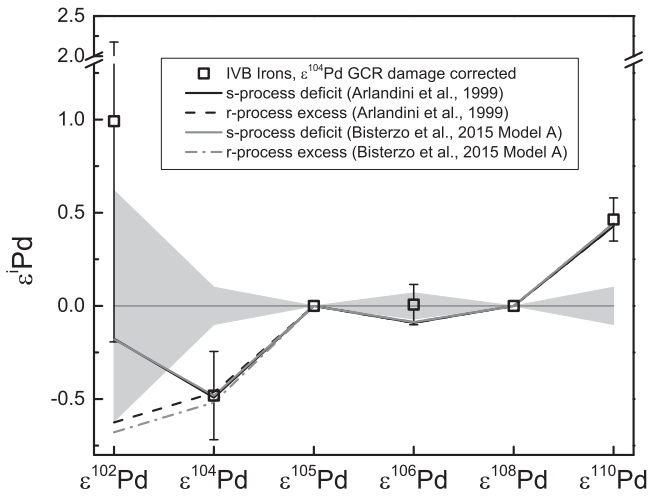


**Figure 7.** Average Pd isotopic composition for 10 IVB iron meteorites;  $\epsilon^{104}\text{Pd}$  after GCR correction (see Figure 5). Open squares represent average IVB irons using an error weighted mean. Gray area around the zero line represents typical within-session reproducibility of the terrestrial standard for each isotope ( $^{105}\text{Pd}$  and  $^{108}\text{Pd}$  are used for mass bias correction and, therefore, by definition, zero) and highlights that isotope anomalies in  $^{104}\text{Pd}$  and  $^{110}\text{Pd}$  are clearly resolved. The solid line indicates expected nucleosynthetic anomalies in Pd due to an s-process deficit of 0.005% and the dashed line due to an r-process excess of 0.005% using s-process yields from Arlandini et al. (1999; black line) and Bisterzo et al. (2015; gray line).

parameters based on uncertainties of the Maxwellian Averaged Cross Sections (MACS) result in differences that are negligible in comparison to the expected anomalies. For example, there is a 10% uncertainty from the MACS (Bao et al. 2000) that affects the estimated yield of  $\epsilon^{104}\text{Pd}$  by  $0.05 \epsilon \text{ u}$ . It should be noted that uncertainties on the solar abundances of the Pd isotopes are annulled by the normalization procedure employed in determining the anomalies. The 10 IVB samples show a positive anomaly in  $\epsilon^{110}\text{Pd}$  of  $0.46 \pm 0.12$  (Figure 7). This positive anomaly is in good agreement with the deficit in  $\epsilon^{104}\text{Pd}$ . For  $\epsilon^{106}\text{Pd}$ , the analytical precision is not sufficient to resolve the small deviation from the reference of about  $0.01 \pm 0.11 \epsilon \text{ u}$  (Figure 7). To judge whether the Pd isotope anomalies are r-process excesses or s-process deficits requires a precise measurement of the p-process only  $\epsilon^{102}\text{Pd}$ , which was not accomplished in the present study. Due to the higher abundances of the p-only isotopes, the precise measurement of the p-process isotopes is easier to perform for Mo isotopes, where it was possible to show that the nucleosynthetic isotope anomalies were s-process deficits (Burkhardt et al. 2011).

In Figure 8, the Pd isotope anomalies are compared with anomalies in Mo (Burkhardt et al. 2011), Ru (Chen et al. 2010), W (Qin et al. 2008; Wittig et al. 2013a; Kruijjer et al. 2014) and Os (Walker 2012; Wittig et al. 2013a). Predictions for resulting s-process deficits or r-process excesses are made using yields from AGB stellar models (Arlandini et al. 1999; Bisterzo et al. 2011) or from GCE models (Bisterzo et al. 2014). Due to the absence of branching points for the s-process pathway through Ru and Pd differences between yields from AGB stellar models (e.g., Arlandini et al. 1999; Bisterzo et al. 2011) and yields from GCE models (e.g., Bisterzo et al. 2014) are negligible. The GCE models predict slightly lower Mo anomalies ( $\sim 0.2 \epsilon \text{ u}$ ) than AGB stellar models that are not currently resolvable. The model curves are calculated by subtracting 0.010%–0.015% or 0.005% s-process yields from two separate models proposed by Bisterzo et al. (2011, 2015)

and from Arlandini et al. (1999). For a given magnitude of the deficit, the isotope anomalies calculated from the various models are indistinguishable for Ru, Pd, W and Os. However, due to the branching at  $^{95}\text{Zr}$ , the yields for the Mo isotopes depend on the rate of the  $^{22}\text{Ne}$ -neutron source (Bisterzo et al. 2015). The recommended stellar rate of the  $^{22}\text{Ne}$ -neutron source (Model B) yields Mo anomalies identical to that obtained from Arlandini et al. (1999), but the Bisterzo et al. (2015) Model A with its  $4\times$  enhanced rate for the  $^{22}\text{Ne}$ -neutron source yields higher  $^{96}\text{Mo}$ , the normalizing s-only isotope in Figure 8 for Mo. This has the effect of diminishing the anomaly in r-only  $^{100}\text{Mo}$  and increasing anomalies in the p-process Mo isotopes (Figure 8). Since such an effect is not observed in the Mo–Ru correlation we conclude that observed nucleosynthetic anomalies in meteorites exclude the  $4\times$  enhanced rate for the  $^{22}\text{Ne}$ -neutron source of the main solar system s-process.

Except for Os, which shows no resolvable anomaly, all observed anomalies could be attributed to an s-deficit with the Ru and Mo anomalies requiring a 0.010%–0.015% s-deficit (Dauphas et al. 2004; Chen et al. 2010; Burkhardt et al. 2011). Figure 8 shows that Pd possesses an s-deficit (0.05%) that is about half of the magnitude observed in Ru and Mo, but similar in magnitude to the anomaly observed in W (Qin et al. 2008; Wittig et al. 2013a). By applying different models in Figure 8, it should also be obvious that varying stellar parameters that control the s-process such as the neutron density or temperature do not explain the observed difference in magnitude of the anomalies between Pd and Ru or Mo. The half-life of  $^{103}\text{Ru}$  (39 days) is less than that of  $^{95}\text{Zr}$  (64 days), so any parameter that reduces the s-process yield at Pd by branching at  $^{103}\text{Ru}$  would significantly perturb the Mo isotope composition. Thus, no individual AGB star, or aggregate of stars, can reproduce the analytical results compiled in Figure 8.

Two sets of hypotheses have been postulated to account for the observation of isotopic anomalies in meteorites and their components. The first set of hypotheses maintains that these anomalies represent lateral or temporal isotopic heterogeneity in the solar accretion disk potentially due to supernovae input (e.g., into the interstellar medium) of the r-process during star formation (e.g., Qian & Wasserburg 2001; Yin et al. 2002; Brennecka et al. 2012) and/or to winds from an AGB star (Vanhala & Boss 2001). The second set of hypotheses exploits the thermal processing of presolar grains in a solar accretion disk that is initially homogeneous at a bulk isotopic scale, to create enhancements or deficits of potential host phases that then impart the observed isotope anomalies to the various meteorites accreted from dust in the disk (Dauphas et al. 2004; Regelous et al. 2008; Trinquier et al. 2009; Burkhardt et al. 2012). These hypotheses will be evaluated using the new Pd isotope data, below.

The classical r-process is now viewed as the combined contributions from multiple neutron-rich astrophysical environments (Lattimer & Schramm 1974; Meyer et al. 1992; Qian & Wasserburg 2001). Previously, r-process yields from core-collapse supernovae were thought to dominate over neutron star mergers (NSM; Argast et al. 2004), but more recent studies estimate that NSM combined with Jet-SN can reproduce the r-process abundances observed in old stars (Wehmeyer et al. 2015). The neutrino wind-driven alpha particle process is regarded as the key r-process site for the synthesis of elements with  $A \leq 100$  (Woosley & Janka 2005; Roberts et al. 2010). However, the neutrino-driven wind models do not

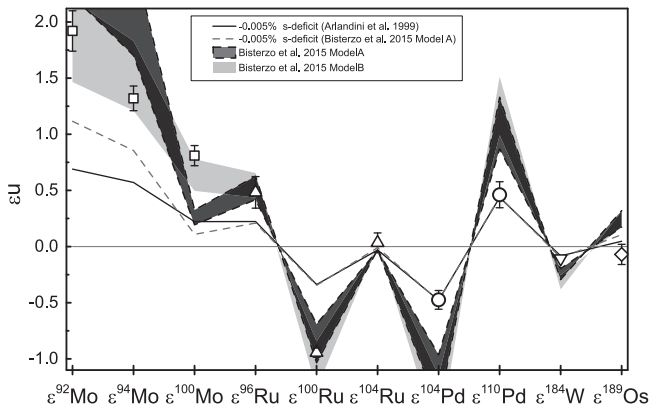


**Figure 8.** Comparison of nucleosynthetic isotope anomalies observed in IVB iron meteorites for Mo (Burkhardt et al. 2011), Ru (Chen et al. 2010), Pd (this study), W (Qin et al. 2008; Wittig et al. 2013a), and Os (Walker 2012; Wittig et al. 2013a) isotopes, together with a prediction for uniform s-process deficits. For Os, data from Warburton Range, that has the least GCR damage, is shown. The solid black line shows the pattern for a 0.005% s-process deficit based on Arlandini et al. (1999) and the dashed gray line is based on the high  $^{22}\text{Ne}(\alpha,n)^{25}\text{Mg}$  production rates in Model A of Bisterzo et al. (2015). Yields for the s-process deficit using model B in Bisterzo et al. (2015) are similar to Arlandini et al. (1999) and are, thus, not shown here. The white band with the solid black line represents an area of predicted nucleosynthetic anomalies caused by 0.010%–0.015% s-process deficits that fits the Mo and Ru data based on Arlandini et al. (1999). The dark gray band with the dashed-dotted line represents a case with high  $^{22}\text{Ne}(\alpha,n)^{25}\text{Mg}$  production rates (model A in Bisterzo et al. 2015) and the light gray band with no lines represents the case with slightly lower  $^{22}\text{Ne}(\alpha,n)^{25}\text{Mg}$  rates (model B in Bisterzo et al. 2015). Note that anomalies based on Arlandini et al. (1999) would fall on the same light gray band. Observed nucleosynthetic Pd isotope anomalies are smaller than those in Mo and Ru, while the predicted effects in Os are too small to clearly resolve.

produce adequate prediction for abundances of  $A > 100$ , critical to the nucleosynthesis of Ru and Pd, due to physical aspects like magnetic fields or rotation that have not been included in the models (Woosley & Janka 2005). Brennecka et al. (2012) observed a distinct break between isotope anomalies in nuclides with  $A < 140$  and higher mass nuclides for Ca–Al-rich inclusions (CAIs) implying that distinct r-process components (e.g., Wasserburg et al. 1996) may have been added to the solar system between the time of formation of CAIs and that of bulk chondrites and planetary bodies. This idea has support from astrophysical observations of old stars containing distinct r-process elemental abundances (e.g., Burris et al. 2000; Sneden & Cowan 2003) and from the distribution of r-process radionuclides ( $^{129}\text{I}/^{182}\text{Hf}$ ) in the solar system (Wasserburg et al. 1996; Qian et al. 1998). However, Lugaro et al. (2014) upwardly revised the s-process yields of  $^{182}\text{Hf}$ , so the ratio  $^{129}\text{I}/^{182}\text{Hf}$  no longer provides evidence of multiple r-process sources.

In this light, the lower slope of the Pd–Mo correlation does not indicate a need for invoking different r-process sites—which are usually assumed to be in the mass region  $A > 110$ ;  $A > 129$  (i.e., L and H events Ott & Kratz 2008; CPR and heavy r-nuclei Qian & Wasserburg 2007)—at lower mass range between Ru and Pd. If Mo and Ru acquired additional r-process contributions from core-collapse supernovae one would see the distinct signature of this r-excess in the isotopic compositions of Mo and Ru. R-process excesses can be distinguished from s-process deficits due to coupling of the r- and p-process anomalies in Mo and Ru that is not observed in the meteoritic anomalies (Chen et al. 2010; Burkhardt et al. 2011). If, on the

other hand, between  $A < 100$  and  $A > 100$  different “r-processes” are accountable for Mo, Ru, and Pd yields iron meteorites might record the observed lower anomaly in Pd in comparison to Mo and Ru. In this context, though, it is important to note, that such r-process is thought to have different r-process yields at  $^{105}\text{Pd}$ ,  $^{106}\text{Pd}$ ,  $^{108}\text{Pd}$ , and  $^{110}\text{Pd}$  (Hoffman et al. 1997; Roberts et al. 2010), than the solar system r-process average (Arlandini et al. 1999; Bisterzo et al. 2011). This would decouple  $\epsilon^{104}\text{Pd}$  and  $\epsilon^{110}\text{Pd}$ , which is not observed in the IVB iron meteorites.

The Pd isotope evidence presented here is a challenge to the first set of models, i.e., heterogeneity in supernovae and AGB star input, since the models predict comparable isotope anomalies in all elements with  $A < 140$ , which includes Mo, Ru and Pd. The offset in the magnitude of the anomaly between Mo–Ru and Pd (Figure 8) is not consistent with a solar system scale variation of  $A < 140$  nuclides versus  $A > 140$  nuclides. From this, we infer that the magnitudes of the nucleosynthetic isotope anomalies in Mo, Ru and Pd are not controlled by the stellar inputs, but must have been affected by subsequent nebular processing.

Bulk meteorites show a correlation of the nucleosynthetic isotope anomalies for the refractory and carbide-forming Ru and Mo (Dauphas et al. 2004; Chen et al. 2010; Burkhardt et al. 2011). The presence of large Ru and Mo isotope anomalies in presolar SiC grains (Nicolussi et al. 1998; Savina et al. 2004) suggests that circumstellar refractory carbides are important carriers of these anomalies. The variations in Ru and Mo nucleosynthetic isotope anomalies of different iron meteorite groups and chondrites have been attributed to the inhomogeneous distribution of their particular (SiC) carrier in the solar nebula (Dauphas et al. 2004). If this were correct, then no Pd isotope anomalies would be predicted to occur in iron meteorites since Pd is not known to form carbides. Kashiv et al. (2002) analyzed trace elements in presolar SiC by synchrotron X-ray fluorescence using a 24.5 keV beam, energetic enough to have excited Pd X-rays (Pd  $K\alpha = 24.35$  KeV). They found Mo and Ru but did not detect Pd, confirming that presolar SiC is not the carrier of Pd isotope anomalies. Further, Pd is not concentrated in refractory-enriched metal (e.g., Campbell et al. 2003). Therefore, processing of SiC or refractory metal carriers cannot account for the relative magnitudes of the nucleosynthetic anomalies in Mo, Ru, and Pd (Figure 8).

Trinquier et al. (2009) observed that correlated isotopic anomalies between nuclides that were created in different astrophysical settings ( $^{54}\text{Cr}$ ,  $^{46}\text{Ti}$ ,  $^{50}\text{Ti}$ ) in bulk chondrites indicated a thermal process imparting selective loss of unstable presolar grains (Trinquier et al. 2009). The observed anomalies in Pd isotopes are consistent with thermal processing of presolar grain carriers that partially obliterated the nucleosynthetic anomalies in Pd relative to those of Mo and Ru. We conclude that the isotope anomalies for elements beyond the Fe peak observed in bulk meteorites are also relicts that reflect solar system processing.

## 5. CONCLUSIONS

The new Pd isotopic compositions reported in this study for IVB irons establish the presence of substantial cosmogenic and nucleosynthetic effects, both of which proved to be of utility. The effects of the reaction  $^{103}\text{Rh}(n, \beta^-)^{104}\text{Pd}$  are well correlated with isotopic effects produced by the reaction  $^{191}\text{Ir}(n, \beta)^{192}\text{Pt}$ . Model cosmogenic anomaly predictions starting

with terrestrial Pd isotopic composition agree with the slopes of the Pd isotopic compositions of IVB irons. Thus, Pd isotopic composition may prove useful as an in situ cosmogenic neutron dosimeter in other irons with sufficiently high Rh/Pd ratios.

The intercepts (Figure 5) reveal the presence of clearly measurable nucleosynthetic effects in the 10 IVB irons reported here, with  $\epsilon^{104}\text{Pd} = -0.48 \pm 0.24$ ,  $\epsilon^{106}\text{Pd} = 0.01 \pm 0.11$ , and  $\epsilon^{110}\text{Pd} = 0.46 \pm 0.12$   $\epsilon$ -units. These nucleosynthetic effects are consistent with s-process deficits, however, the magnitude of the isotope anomaly in Pd is about half that observed in Mo and Ru. Increasing the rate of the  $^{22}\text{Ne}(\alpha, n)^{25}\text{Mg}$ -neutron source rate used by Bisterzo et al. (2015; Model A) gives s-process results that are not consistent with the observed Mo–Ru–Pd isotopic anomalies. The observed Mo–Ru–Pd relationship implies that nebular processing of the presolar carriers must have selectively reduced the anomaly due to the less refractory character of Pd carriers, either metal or sulfides. The presence of a nucleosynthetic isotope anomaly in Pd demonstrates that isotope anomalies are not restricted to exclusively refractory elements, but must have been pervasive for all elements with  $A > 60$  between planetary bodies in the early solar system. The new Pd isotope data imply that the survival of isotope anomalies is controlled, at least partially, by the properties of the element and that the chemical processing experienced by (presolar) dust in the early solar system appears to control the magnitude of the observable anomalies. Elements that occur in chemically volatile phases (e.g., Fe, Zn, Cu; Moynier et al. 2007) are unlikely to exhibit nucleosynthetic anomalies at the planetary scale, while Ni (Regelous et al. 2008) and Pd (this study) retained nucleosynthetic isotope anomalies.

This research was supported by the Cosmochemistry Program of the National Aeronautics and Space Administration (NNX13AI06G) and by the Swiss National Science Foundation (SNF). We thank Jim Chen for early discussions on the difficulties of dealing with interferences on Pd isotopic composition. We thank Glenn MacPherson, Linda Welzenbach and Tim McCoy (NMNH), Denton Ebel and Joe Boesenberg (AMNH), Rhiannon Mayne (Oscar G. Monnig Collection, Texas Christian University), Lora Bleacher (Center for Meteorite Studies, Arizona State University), and Carl Francis (Harvard Mineralogical Museum) for supplying samples. The manuscript benefitted thoroughly from input by an anonymous reviewer.

## REFERENCES

- Akram, W., Schönbachler, M., Bisterzo, S., & Gallino, R. 2015, *GCA*, 165, 484
- Argast, D., Samland, M., Thielemann, F.-K., & Qian, Y.-Z. 2004, *A&A*, 416, 997
- Arlandini, C., Kappeler, F., Wisshak, K., et al. 1999, *ApJ*, 525, 886
- Bao, Z. Y., Beer, H., Käppeler, F., et al. 2000, *ADNDT*, 76, 70
- Bisterzo, S., Gallino, R., Kappeler, F., et al. 2015, *MNRAS*, 449, 506
- Bisterzo, S., Gallino, R., Straniero, O., Cristallo, S., & Käppeler, F. 2011, *MNRAS*, 418, 284
- Bisterzo, S., Travaglio, C., Gallino, R., Wiescher, M., & Käppeler, F. 2014, *ApJ*, 787, 10
- Brennecka, G. A., Borg, L. E., & Wadhwa, M. 2012, in 43rd LPSC (Houston, TX: Lunar and Planetary Institute), 2006 <http://www.lpi.usra.edu/meetings/lpsc2012/pdf/2006.pdf>
- Burkhardt, C., Kleine, T., Dauphas, N., & Wieler, R. 2012, *EPSL*, 357, 298
- Burkhardt, C., Kleine, T., Oberli, F., et al. 2011, *EPSL*, 312, 390
- Burris, D. L., Pilachowski, C. A., Armandroff, T. E., et al. 2000, *ApJ*, 544, 302
- Campbell, A. J., & Humayun, M. 2005, *GCA*, 69, 4733
- Campbell, A. J., Simon, S. B., Humayun, M., & Grossman, L. 2003, *GCA*, 67, 3119
- Carlson, R. W., Boyet, M., & Horan, M. 2007, *Sci*, 316, 1175
- Chen, J. H., Papanastassiou, D. A., & Wasserburg, G. J. 2010, *GCA*, 74, 3851
- Dauphas, N., Davis, A. M., Marty, B., & Reisberg, L. 2004, *EPSL*, 226, 465
- Hoffman, R. D., Woosley, S. E., & Qian, Y.-Z. 1997, *ApJ*, 482, 951
- Kashiv, Y., Cai, Z., Lai, B., et al. 2002, in 33rd LPSC (Houston, TX: Lunar and Planetary Institute), 2056 <http://www.lpi.usra.edu/meetings/lpsc2002/pdf/2056.pdf>
- Kelly, W. R., & Wasserburg, G. J. 1978, *GeoRL*, 5, 1079
- Kruijer, T. S., Fischer-Gödde, M., Kleine, T., et al. 2013, *EPSL*, 361, 162
- Kruijer, T. S., Touboul, M., Fischer-Gödde, M., et al. 2014, *Sci*, 344, 1150
- Lattimer, J. M., & Schramm, D. N. 1974, *ApJL*, 192, L145
- Leya, I., & Masarik, J. 2013, *M&PS*, 48, 665
- Leya, I., Wieler, R., & Halliday, A. N. 2000, *EPSL*, 175, 1
- Leya, I., Wieler, R., & Halliday, A. N. 2003, *GCA*, 67, 529
- Lodders, K. 2003, *ApJ*, 591, 1220
- Lugaro, M., Heger, A., Osrin, D., et al. 2014, *Sci*, 345, 650
- Markowski, A., Leya, I., Quitté, G., et al. 2006a, *EPSL*, 250, 104
- Markowski, A., Quitté, G., Halliday, A. N., & Kleine, T. 2006b, *EPSL*, 242, 1
- Masarik, J. 1997, *EPSL*, 152, 181
- Meyer, B. S., Mathews, G. J., Howard, W. M., Woosley, S. E., & Hoffman, R. D. 1992, *ApJ*, 399, 656
- Moynier, F., Blichert-Toft, J., Telouk, P., Luck, J.-M., & Albarède, F. 2007, *GCA*, 71, 4365
- Mughabghab, S. F. 2003, in IAEA INIS Collection (Vienna: IAEA), 1 [https://inis.iaea.org/search.aspx?orig\\_q=RN:34020739](https://inis.iaea.org/search.aspx?orig_q=RN:34020739)
- Nicolussi, G. K., Pellin, M. J., Lewis, R. S., & Davis, A. M. 1998, *ApJ*, 504, 492
- Ott, U., & Kratz, K.-L. 2008, *NewAR*, 52, 396
- Qian, Y.-Z., Vogel, P., & Wasserburg, G. J. 1998, *ApJ*, 494, 285
- Qian, Y.-Z., & Wasserburg, G. J. 2001, *ApJ*, 567, 515
- Qian, Y.-Z., & Wasserburg, G. J. 2007, *PhR*, 442, 237
- Qin, L., Dauphas, N., Wadhwa, M., Masarik, J., & Janney, P. E. 2008, *EPSL*, 273, 94
- Regelous, M., Elliott, T., & Coath, C. D. 2008, *EPSL*, 272, 330
- Roberts, L. F., Woosley, S. E., & Hoffman, R. D. 2010, *ApJ*, 722, 954
- Savina, M. R., Davis, A. M., Tripa, C. E., et al. 2004, *Sci*, 303, 649
- Schönbachler, M., Carlson, R. W., Horan, M. F., Mock, T. D., & Hauri, E. H. 2008, *GCA*, 72, 5330
- Snedden, C., & Cowan, J. J. 2003, *Sci*, 299, 70
- Trinquier, A., Elliott, T., Ulfbeck, D., et al. 2009, *Sci*, 324, 374
- Vanhala, H. a. T., & Boss, A. P. 2001, *ApJ*, 575, 1144
- Voshage, H. 1984, *EPSL*, 71, 181
- Walker, R. J. 2012, *EPSL*, 351-352, 36
- Walker, R. J., McDonough, W. F., Honesto, J., et al. 2008, *GCA*, 72, 2198
- Wasserburg, G. J., Busso, M., & Gallino, R. 1996, *ApJL*, 466, L109
- Wehmeyer, B., Pignatari, M., & Thielemann, F.-K. 2015, *MNRAS*, 452, 1970
- Wittig, N., Humayun, M., Brandon, A. D., Huang, S., & Leya, I. 2013a, *EPSL*, 361, 152
- Wittig, N., Humayun, M., & Leya, I. 2013b, in 44th LPSC (Houston, TX: Lunar and Planetary Institute), 2355 <http://www.lpi.usra.edu/meetings/lpsc2013/pdf/2355.pdf>
- Woosley, S., & Janka, T. 2005, *NatPh*, 1, 147
- Yin, Q.-Z., Jacobsen, S. B., & Yamashita, K. 2002, *Natur*, 415, 881